Ventromedial prefrontal parvalbumin neurons are necessary for initiating cued threat avoidance

Yi-Yun Ho[1,2], Qiuwei Yang[1], Priyanka Boddu[1], David A. Bulkin[1,2], Melissa R. Warden[1,2,*]

[1]Department of Neurobiology and Behavior, Cornell University, Ithaca, NY 14853, USA.
[2]Cornell Neurotech, Cornell University, Ithaca, NY 14853, USA.

*Corresponding author: mrwarden@cornell.edu

ABSTRACT

The ventromedial prefrontal cortex (vmPFC) is essential for regulating the balance between reactive and adaptive response. Reactive, hard-wired behaviors – such as freezing or flight – are feasible in some situations, but in others contexts an acquired, adaptive action may be more effective. Although the vmPFC has been implicated in adaptive threat avoidance, the contribution of distinct vmPFC neural subtypes with differing molecular identities and wiring patterns is poorly understood. Here, we studied vmPFC parvalbumin (PV) interneurons in mice as they learned to cross a chamber in order to avoid an impending shock, a behavior that requires both learned, adaptive action and the suppression of cued freezing. We found that vmPFC PV neural activity increased upon movement to avoid the shock, when the competing freezing response was suppressed. However, neural activity did not change upon movement toward cued rewards or during general locomotion, conditions with no competing behavior. Optogenetic suppression of vmPFC PV neurons delayed the onset of avoidance behavior and increased the duration of freezing, but did not affect movement toward rewards or general locomotion. Thus, vmPFC PV neurons support flexible, adaptive behavior by suppressing the expression of prepotent behavioral reactions.

INTRODUCTION

The prefrontal cortex is essential for the execution of purposeful, goal-directed behaviors (Duncan, 1986; Miller and Cohen, 2001). Pursuing an intended goal requires suppressing immediate reactions that conflict with future-directed behaviors, and hallmarks of prefrontal damage in humans and animals include stimulus-bound and context-inappropriate behaviors, excessive reactivity, and impulsivity (Bianchi, 1922; Lhermitte, 1983). Although innate, reactive behaviors – such as freezing or flight – are applicable in some situations, in others an acquired, adaptive action may be more effective. The ventromedial prefrontal cortex (vmPFC), including the infralimbic cortex and dorsal peduncular cortex, is specialized for supporting the adaptive action by suppressing immediate reactions (Hardung et al., 2017; Murphy et al., 2005), and plays a critical role in fear extinction (Do-Monte et al., 2015; Milad and Quirk, 2002) and active avoidance (Halladay and Blair, 2017; Moscarello and LeDoux, 2013).

Parvalbumin (PV) neurons in the vmPFC synapse onto and inhibit local pyramidal neurons. Although we might expect that activation of vmPFC PV neurons would release reactive behaviors such as freezing by suppressing vmPFC outputs, the relationship between PV and pyramidal neuron firing is complex. Cortical PV neurons have been reported to activate simultaneously with local pyramidal neurons (Estebanez et al., 2017; Giordano et al., 2021; Isomura et al., 2009;

Merchant et al., 2008; Nashef et al., 2020; Okun and Lampl, 2008; Pinto and Dan, 2015), and it has been suggested that PV neurons may help to shape, rather than gate, the firing of local pyramidal neurons (Isomura et al., 2009; Merchant et al., 2012).

The question thus arises whether the activation of vmPFC PV neurons suppresses or facilitates reactive behavior. To address this, we probed the role of vmPFC PV neurons during active avoidance behavior in mice. During active avoidance, animals first freeze in response to shock-predicting tones, as in fear conditioning, but gradually learn that they can avoid the shock by crossing the chamber when a tone plays. This behavior requires both the suppression of cued freezing and an adaptive movement toward a safe zone (Koolhaas et al., 1999; Krypotos et al., 2015; Moscarello and LeDoux, 2014, 2013; Mowrer and Lamoreaux, 1946), and is desirable for this study since both reactive and deliberate behavior can be observed in a single trial. Using fiber photometry, we show that vmPFC PV neuron activity increases specifically when mice move to avoid a future shock, but does not increase when animals move to obtain a cued reward or move in a neutral context. Further, we show that optogenetic suppression of vmPFC PV neural activity prolongs freezing and delays avoidance, but does not affect movement toward cued rewards or general locomotion. These results reveal that vmPFC PV neurons play an essential and counterintuitive role in supporting adaptive behavior, and suggests a role for PV neurons in shaping vmPFC function that goes beyond suppression.

RESULTS

vmPFC PV neural activity is elevated at avoidance

We first asked whether and how vmPFC PV neurons respond during the freezing-to-avoidance transition. To target this population for recording, we selectively expressed a genetically encoded calcium indicator, GCaMP6f, in vmPFC PV neurons by locally injecting a Cre-dependent viral vector (AAV-CAG-Flex-GCaMP6f) into the vmPFC of PV-Cre mice. In control mice, we expressed GFP in PV neurons by injecting AAV-CAG-Flex-GFP. We implanted an optical fiber over the vmPFC to monitor calcium-dependent fluorescence, and recorded vmPFC PV population activity via fiber photometry (**Figure 1A,B**) (Cui et al., 2013; Gunaydin et al., 2014).

To study the transition from freezing to avoidance we used a two-way signaled active avoidance paradigm (**Figure 1C**). An auditory cue (constant tone at 12 kHz or 8 kHz) was played, and to avoid an impending foot shock the mouse had to cross the midline of the behavioral testing chamber within 5 seconds of tone onset. If the mouse crossed the chamber during this 5-second

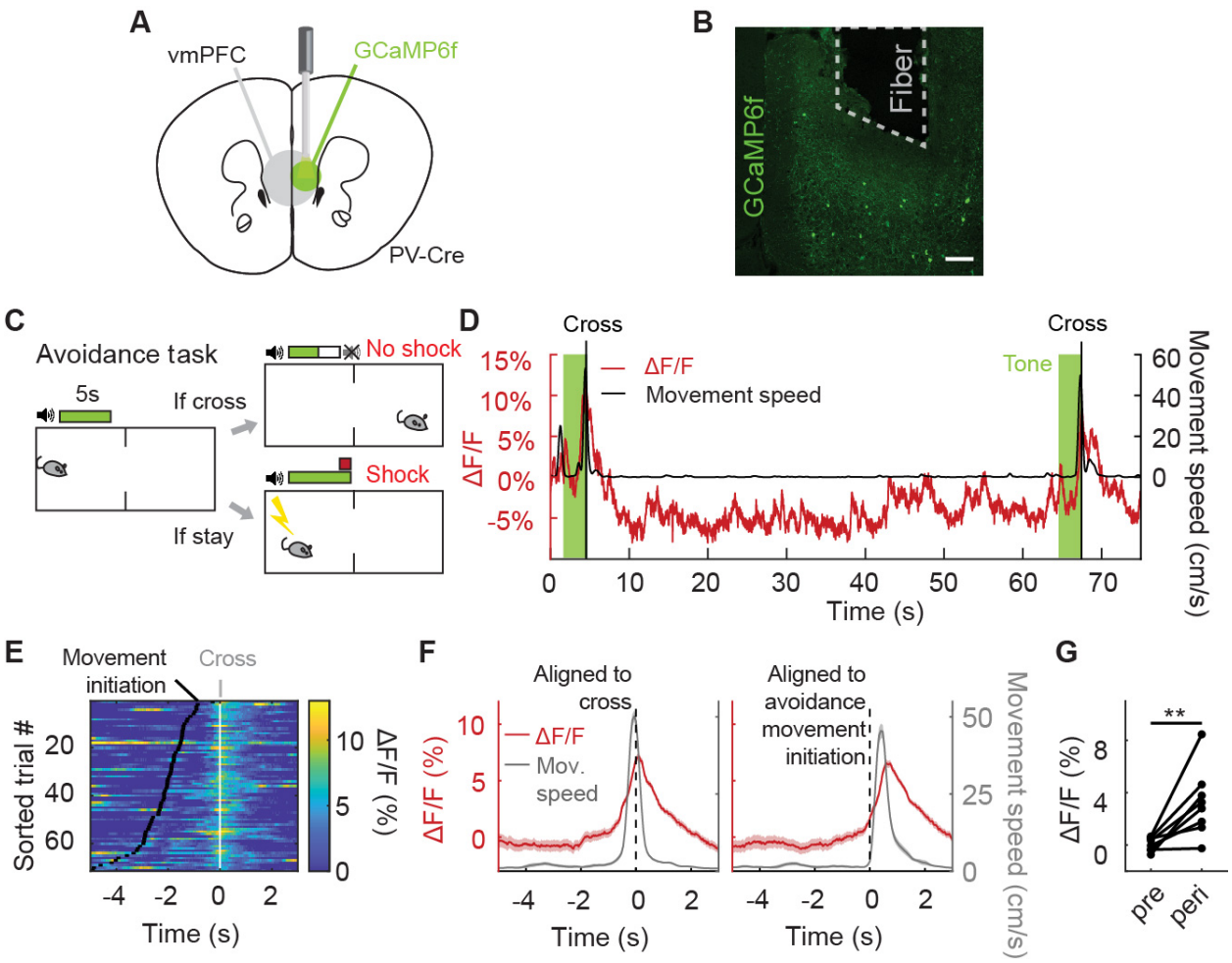

Figure 1. vmPFC PV signals active avoidance
(A) Fiber photometry schematic. (B) GCaMP6f expression in vmPFC PV neurons. Scale bar, 100 μm. (C) Active avoidance task schematic. The green box indicates presence of the tone, which lasts till animal crosses. (D) Example vmPFC PV ΔF/F (red) and speed (black) during two successful avoidance trials. Vertical line indicates chamber crossing. Tone, light green. (E) vmPFC PV ΔF/F during successful avoidance trials, data aligned to chamber crossing. White ticks: chamber crossing. Black ticks: tone onset. Same example mouse as D. (F) Example average vmPFC PV ΔF/F (red) and speed (grey), aligned to chamber crossing (left) and movement initiation (right). Same example mouse as D. (G) Average vmPFC PV ΔF/F before chamber crossing (pre, 4 to 2 seconds before cross) and during chamber crossing (peri, 1 second before to 1 second after crossing) (N = 8 mice). **$p < 0.01$, paired t-test. Shaded regions indicate SEM.

period, and so avoided the foot shock and terminated the tone, the trial was scored as a successful avoidance trial. If the mouse failed to cross the chamber during this period a 2 second foot shock was delivered. Mice could terminate the foot shock early by crossing the chamber, which was scored as an escape. The tone terminated at either avoidance or shock offset. Prior to avoidance training, mice received two tone-shock pairings to learn the association between the auditory cue and the foot shock.

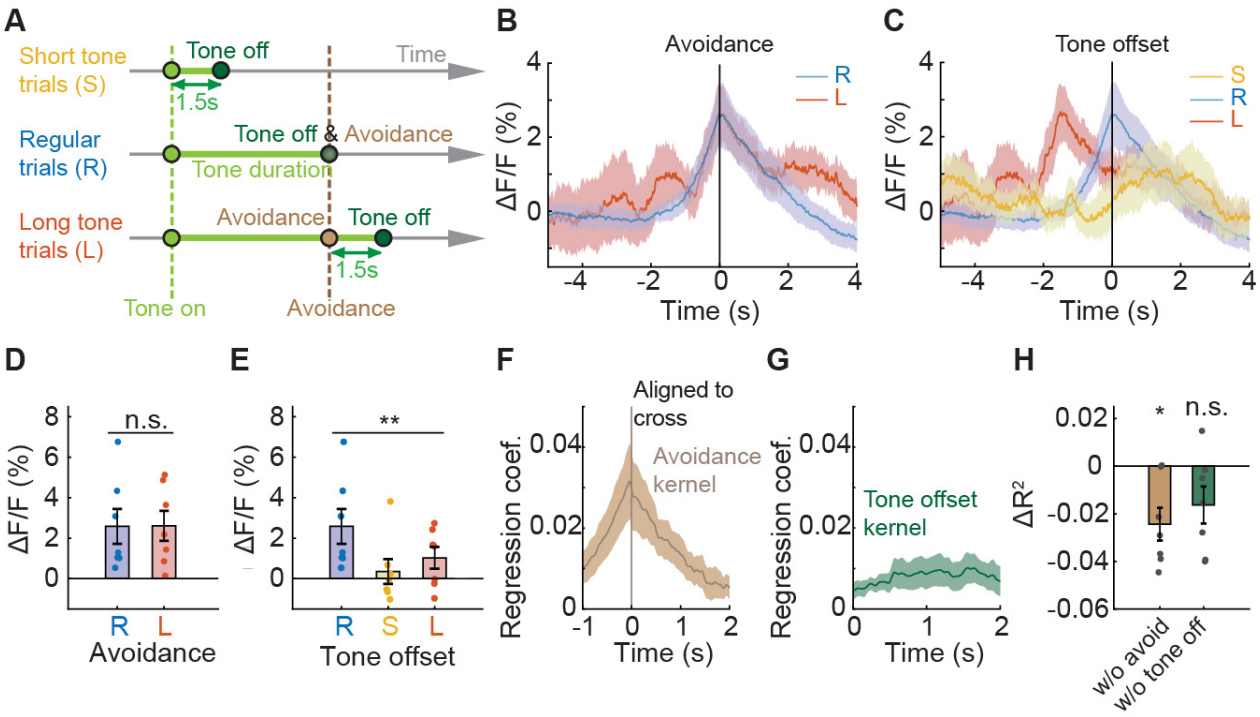

Figure 2. vmPFC PV neural activity reflects the avoidance movement, not the predictive tone
(A) Schematic of a modified version of avoidance task including 10% short tone trials (S), where tone only lasts for 1.5 seconds regardless of animal's action,10% long tone trials (L), where the tone lasts until 1.5 seconds after a successful avoidance, and 80% regular trials (R). (B-C) Average vmPFC PV ΔF/F aligned to (B) chamber crossing and (C) tone offset (N = 7 mice). S: short tone trials; R: regular trials; L: long tone trials. (D) Comparison between average vmPFC PV calcium activity between 0 to 0.1 seconds after avoidance chamber crossings in regular trials (R) and long tone trials (L). Each circle mark indicates average calcium activity across trials of one animal. (E) Comparison among average vmPFC PV calcium activity between 0 to 0.1 seconds after tone offsets in regular trials (R), short tone trials (S), and long tone trials (L). Each circle mark indicates average calcium activity across trials of one animal. (F-G) Average avoidance kernel (F) and average tone offset kernel (G) across all animals (N=7 mice) calculated by a linear model. (H) Loss of predictive power (ΔR^2) in a reduced model with shuffled avoidance or tone offset time points. n.s. $p>0.05$, *$p < 0.05$, **$p < 0.01$, (D): one-way repeated measure ANOVA, (E): paired t-test, (H): one-sample t-test. Error bars indicate SEM. Shaded regions indicate SEM.

As vmPFC inactivation impairs avoidance behavior (Halladay and Blair, 2017; Moscarello and LeDoux, 2013), the activity of inhibitory vmPFC PV neurons might be predicted to be low during successful avoidance trials. Intriguingly, we found that vmPFC PV neural activity rose upon the initiation of avoidance movements and peaked at chamber crossing (**Figure 1D-G**, $p < 0.01$, paired t-test; **Figure 1—Figure supplement A-E**). The trial-by-trial variability in the amplitude of vmPFC PV neural activity was not correlated with variability in the speed or latency of the avoidance movement (**Figure 1—Figure supplement F-K**).

During successful avoidance trials, two events happen simultaneously: the mouse crosses the chamber, and a shock-predicting tone is terminated. To determine whether PV neural activity better reflects the avoidance movement or the termination of the predictive auditory cue, we designed a version of the avoidance task with additional trial types to uncouple these events. Regular trials (80%) were interleaved with trials with shortened (10%) or lengthened (10%) tones (**Figure 2A**). In short-tone trials the tone lasted for only 1.5 seconds, and in long-tone trials the tone was not terminated until 1.5 seconds after successful avoidance (**Figure 2A**). vmPFC PV neural activity at chamber crossing did not differ between regular and long-tone trials (**Figure 2B,D**, $p > 0.05$, paired t-test), but PV neural activity at tone offset was significantly different among short-tone, regular, and long-tone trials (**Figure 2C,E**, $p < 0.01$, one-way repeated ANOVA). Short-tone trials were not included in the chamber crossing analysis because there usually was no chamber crossing in these trials, but the mouse could not distinguish between regular and long-tone trials until after crossing.

We extracted characteristic neural responses to each event without interference from other events close in time. We constructed a linear regression model to extract the isolated neural responses to chamber crossing and tone termination (Musall et al., 2019; Parker et al., 2016), and all major events were included in the model. We assumed (1) that neural responses would be similar for the same events and dissimilar for different events, and (2) neural responses to events can be summed up linearly to form the recorded signals. With these assumptions and through linear regression, isolated neural responses to each event were extracted. The model-extracted isolated neural response to tone offset was flat, while the isolated avoidance signal peaked at chamber crossing (**Figure 2F,G**). To further demonstrate that vmPFC PV activity can be better accounted for by the action to avoid the shock than tone termination, we compared the explanatory power (R^2, coefficient of determination) of the reduced model with shuffled time points to the full model. Shuffling the avoidance time points significantly reduced the explanatory power of the model (ΔR^2 different from zero, $p < 0.05$, one-sample t-test), while shuffling the tone offset time points had no effect ($p > 0.05$, one-sample t-test, **Figure 2H**). Thus, vmPFC PV neural activity at chamber crossing reflects the avoidance behavior and not the cessation of the predictive auditory cue.

vmPFC PV neural activity does not reflect movement to obtain rewards

vmPFC PV neural activity rises during movement to avoid a predicted future shock (see time = 0 in **Figure 1E,F**), but it is unclear whether this neural activity specifically reflects avoidance, or if vmPFC PV neural activity would be elevated during any movement. If vmPFC PV neural activity

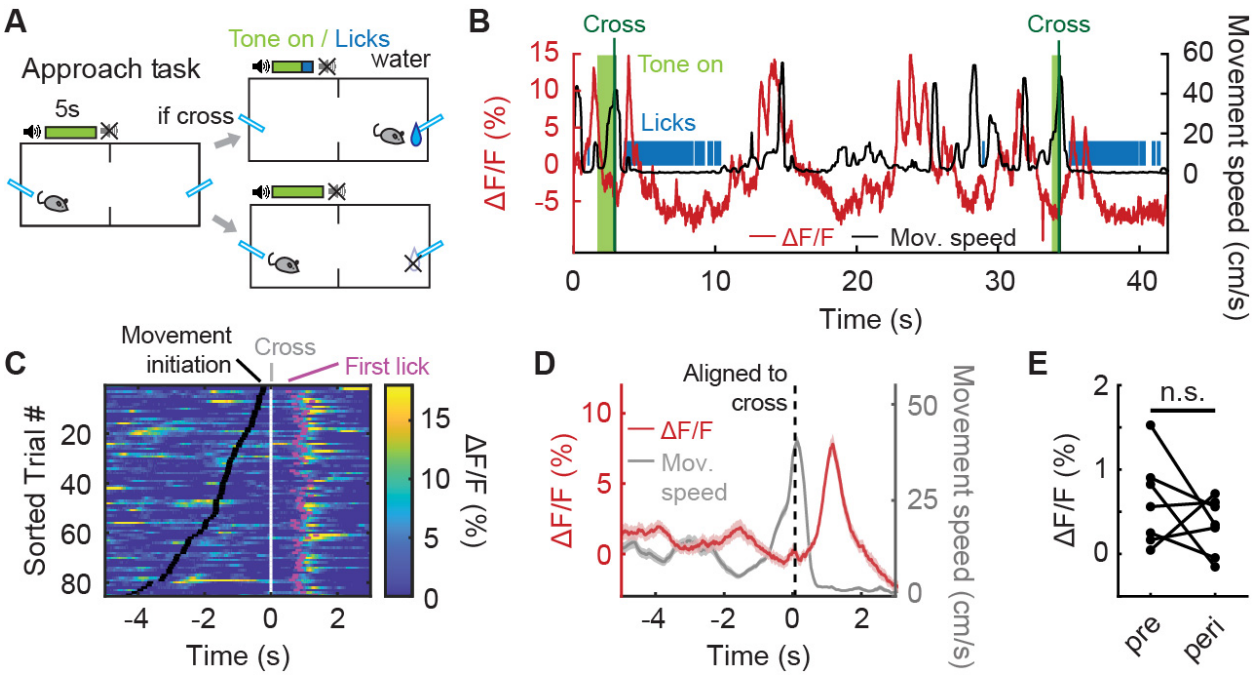

Figure 3. vmPFC PV activity does not signal reward-approach movements during reward seeking behavior.
(A) Reward approach task schematic. (B) Example vmPFC PV ΔF/F (red) and speed (black) during two successful approach trials. Vertical line indicates chamber crossing. Tone, light green. (C) vmPFC PV ΔF/F during successful approach trials, data aligned to chamber crossing. Black ticks: tone onset, white ticks: chamber crossing, magenta ticks: licks. Same example mouse as B. See Figure 1E for comparison, wherein vmPFC PV are active at crossing (time = 0) during active avoidance task. (D) Example average vmPFC PV ΔF/F (red) and speed (grey), aligned to chamber crossing (left). Same example mouse as B. See Figure 1F for comparison, wherein vmPFC PV are active at crossing (time = 0) during active avoidance task. (E) Average vmPFC PV ΔF/F before chamber crossing (pre, 4 to 2 seconds before cross) and during chamber crossing (peri, 1 second before to 1 second after crossing) (N = 7 mice). n.s. $p > 0.05$, paired t-test. Shaded regions indicate SEM.

reflects locomotor activity, we would expect to see elevated neural activity during movement to obtain rewards, and during movement in the open field. To test this idea, we recorded vmPFC PV neuronal activity during a reward approach task, which mirrored the avoidance design in temporal structure, but shock omission on successful chamber crossing was replaced with reward delivery (**Figure 3A**). In this task, chamber-crossing movements to obtain a water reward were not associated with elevated vmPFC PV neural activity (**Figure 3B-E**, $p > 0.05$, paired t-test; **Figure 3—Figure supplement A**; see **Figure 1C-G** for comparison).

We observed an elevation of vmPFC PV neuronal activity after chamber crossing when the animals started to consume the water reward (**Figure 3C**, magenta dots, and **Figure 3D**). To test whether this transient increase in vmPFC PV neuron activity after chamber crossing reflects water consumption or the preceding approach behavior, we introduced randomized water-omission

trials in 10% of the trials (**Figure 3—Figure supplement B-D**). We found that the PV neuron signal was flat when the water reward was omitted (**Figure 3—Figure supplement C**). Increases of vmPFC PV activity were well-aligned to the first lick to consume water reward delivered after a successful crossing (**Figure 3—Figure supplement D**). These results indicated that vmPFC PV neurons do not respond to a motivated reward-approach action but rather to water consumption, where animals stopped foraging and paused for reward consumption. Overall, these results demonstrate that vmPFC PV neuronal activity does not respond to every goal-directed action.

To further demonstrate that the elevated vmPFC PV neuronal activity we saw during avoidance did not merely reflect locomotion, we recorded vmPFC PV activity in an open field test (OFT), where animals were allowed to run freely without any defined task structure (**Figure 3—Figure supplement E,F**). When we aligned vmPFC PV activity to movement peaks, no elevated activity was observed (**Figure 3—Figure supplement G**). We varied the overhead lighting and found that vmPFC PV neurons showed no elevated activity during movement under either a bright ceiling light, which is a more aversive setting to the mice, or a dim ceiling light, which is more comforting to the mice (**Figure 3—Figure supplement 3H,I**, bright light: $p = 0.8705$, dim light: $p = 0.1475$, paired t-test; **Figure 3—Figure supplement J**). It should be noted that the OFT is a relatively neutral context, regardless of lighting conditions, when compared to the appetitive reward approach or aversive active avoidance.

vmPFC PV becomes positively correlated to movement after shock

One difference between the avoidance, approach, and open field tasks is environmental valence, and in differently-valenced environments animals engage in different suites of behaviors. For example, animals in moderately threatening environments spend less time exploring than animals in rewarding positively correlated to movement when animals are requires to suppress the expression of an environment-specific prepotent behavior. Active avoidance is associated with two underlying behavioral components: an initial freeze in response to the shock-predicting cue, and a chamber-crossing movement to prevent the shock. Animals first learn the association between the tone and the shock, and freeze in response to the tone, but eventually learn to suppress this freeze in order to prevent the shock. In contrast, when animals are engaged in reward-based tasks, there is no conflicting action to suppress.

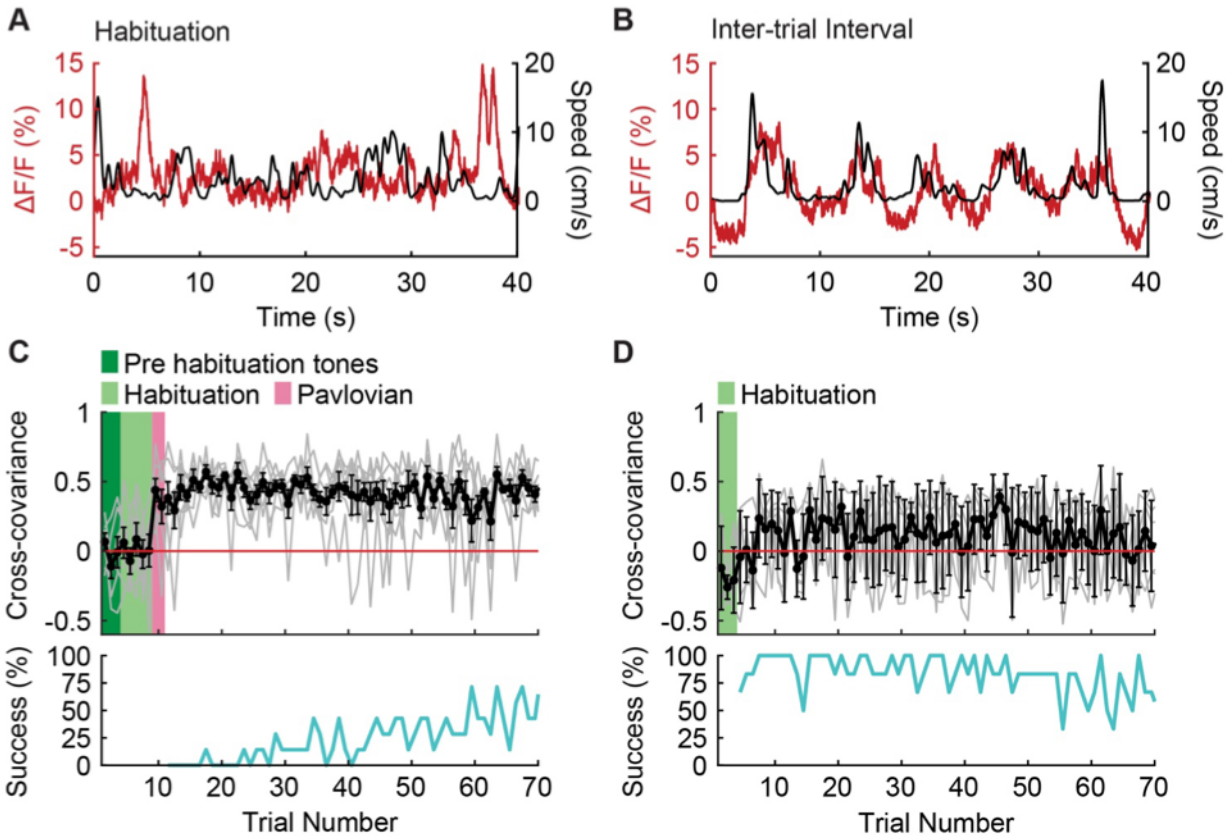

Figure 4. vmPFC PV activity becomes correlated to movement after shock.
(A-B) Example vmPFC PV ΔF/F (red) and speed (black) during (A) habituation prior to the first-ever shock exposure, and (B) the inter-trial interval after avoidance training. (C-D) Evolution of cross-covariance between vmPFC PV activity and speed over trials (upper panel, black) and corresponding average avoidance success rate across animals (bottom panel, cyan) on (C) the first day of avoidance training (N = 7 mice) and (D) in a well-learned phase in approach (N = 6 mice). Error bars indicate SEM.

To test this hypothesis, we analyzed the recordings made on the first day of active avoidance training to determine how movement-related vmPFC PV neural activity evolves over learning. On the first session, we habituated the animals to the chamber for 5 minutes before the task started. During this habituation period, vmPFC PV activity was not positively correlated with movement (**Figure 4A; Figure 4—Figure supplement A**), similar to our observations in appetitive and neutral contexts (**Figure 3; Figure 3—Figure supplement E-I**). As avoidance training progressed, we found that vmPFC PV activity became elevated during movements in the inter-trial interval (**Figure 4B; Figure 4—Figure supplement A**). Considering that animals minimize their movements in threatening environments, movement outside of the tone-evoked trial could require suppression of this natural inclination. This correlation between movement and vmPFC PV neural activity during the inter-trial interval did not emerge until after animals experienced the

first foot shock (**Figure 4C; Figure 4—Figure supplement A**). The correlation between movement and vmPFC PV neuronal activity emerged immediately after receiving the first shock and did not increase during the learning process, suggesting that avoidance learning is not necessary for the correlation between movement and vmPFC PV neural activity to emerge. The lack of positive correlation between activity and movement in the habituation phase (**Figure 4A-C; Figure 4—Figure supplement A**) of the avoidance task is similar to what was observed throughout the approach task (**Figure 4D; Figure 4—Figure supplement B**). These data show that the positive correlation between movement and PV neuron activity only emerges after animals learn that their current environment is threatening, and movement requires a suppression of the prepotent behavioral freezing state.

Inhibiting vmPFC PV activity delays avoidance

To investigate the causal role of vmPFC PV neural activity in active avoidance, we bilaterally inhibited vmPFC PV neurons by expressing Cre-dependent halorhodopsin (AAV5-EF1α-DIO-eNpHR; control animals: AAV5-EF1α-DIO-eYFP) in PV-Cre mice (**Figure 5A,B**). We used the same avoidance and approach tasks described above (**Figure 1A; Figure 3A**), and introduced interleaved simulation blocks where vmPFC PV neurons were optogenetically inhibited during the interval from 0.5 to 2.5 seconds after tone onset (**Figure 5C**). Inhibiting vmPFC PV neuronal activity delayed the avoidance movement (**Figure 5D-G; Figure 5—Figure supplement A,B**; **Video 1**) but did not delay the movement for water reward in the approach task (**Figure 5H-K; Figure 5—Figure supplement C,D**) or the speed of voluntary locomotion in the OFT (**Figure 5L-O**, dim OFT: interaction between opsins and stimulation: $p = 0.7636$, 2-way ANOVA; bright OFT: interaction between opsins and stimulation: $p = 0.7469$, 2-way ANOVA).

Both the speed of the avoidance movement (**Figure 5D,E**, significant interaction between opsin and stimulation, $p = 0.0281$, 2-way ANOVA) and the probability of successful avoidance (**Figure 5F,G**, $p = 0.0058$, unpaired t-test) were reduced by suppression of vmPFC PV neurons. The speed of movement and the probability of successful reward delivery were not affected in the reward approach task (speed: **Figure 5H,I**, interaction between opsin and stimulation, $p = 0.479$, 2-way ANOVA; probability of approach: **Figure 5J,K**, $p = 0.1204$, unpaired t-test). This suggests that vmPFC PV neuronal activity is not merely modulated by the avoidance behavior but plays a causal role. By further analyzing the video data, we found that not only the onset of avoidance was delayed, but also that freezing during tone presentation increased (**Figure 5—Figure supplement E-G**, $p = 0.0175$, unpaired t-test; **Video 1**). In addition, the ratio of freezing duration

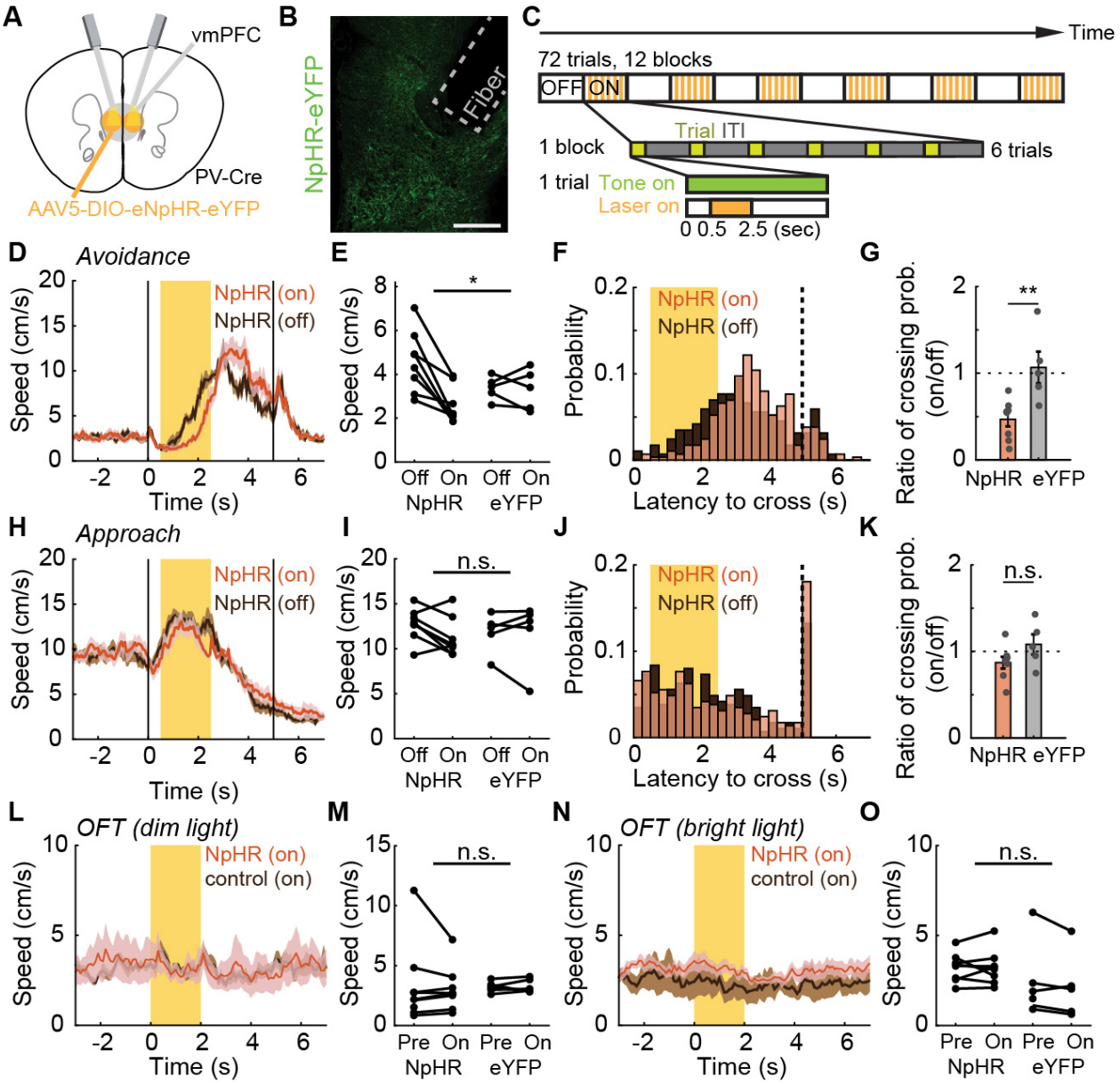

Figure 5. Suppressing vmPFC PV neurons delays avoidance.
(A) Optogenetic schematic. (B) NpHR-eYFP expression in vmPFC PV neurons in a PV-Cre mouse. Scale bar: 200 μm. (C) Optogenetic inactivation schematic. Interleaved simulation blocks were introduced, where vmPFC PV neurons were optogenetically inhibited during the interval from 0.5 to 2.5 seconds after tone onset. (D) Speed of NpHR-expressing mice during avoidance with (red) and without (dark brown) illumination. (E) Speed of NpHR- and eYFP-expressing mice, averaged over the laser stimulation period, with and without illumination. (F) Distribution of crossing latencies during avoidance in NpHR-expressing animals with (red) and without illumination (brown). (G) Ratio of illuminated/non-illuminated chamber crossing probabilities. (H-K) Same as (D-G) for approach task. (L-M) Same as (D-E) but for OFT with dim light. (N-O) Same as (L-M) but for OFT with bright light. *$p < 0.05$, **$p < 0.01$. For (E), (I), (M), and (O), 2-way ANOVA interaction term. For (G) and (K), unpaired t-test. Shaded regions indicate SEM. NpHR: N=8 mice, eYFP: N=5 mice.

to avoidance latency increased during vmPFC PV inhibition (**Figure 5—Figure supplement H**, p

= 0.0302, unpaired t-test; **Video 1**), suggesting that increased avoidance latency was primarily due to an increase in freezing. This finding supports the idea that vmPFC PV promotes avoidance by suppressing the prepotent freezing behavior (Hardung et al., 2017; Murphy et al., 2005).

The finding that vmPFC PV neural activity peaked at both reward delivery and successful shock avoidance raised the question of whether vmPFC PV neuronal activity is also necessary for evaluating the outcomes of current action by increasing activity after good outcomes. If vmPFC PV neuronal activity signals good outcomes, and if the evaluation signals are necessary for learning and for modifying future behavior, we would expect that inhibiting vmPFC PV neuronal activity would not have an immediate effect on performance during the current trial but would affect success in subsequent trials. We first examined this hypothesis in the task described in **Figure 5C**. We found that suppressing vmPFC PV neurons delayed avoidance even on the first trial of a stimulation block. The latency of the first trial of all inhibition blocks is significantly longer than the latency of all pre-stimulation off trials (**Figure 5—Figure supplement I,J,** p = 0.0022,

Video 1. Suppressing vmPFC PV neurons delays avoidance and prolongs freezing
The video displayed the mouse's behavior in response to shock-predicting cues without suppression of vmPFC PV neurons (as shown in the clip "avoidance without stimulation") and with suppression of vmPFC PV neurons (as shown in the clip "avoidance with vmPFC PV suppression"). The shock-predicting cues were on when the caption "Tone on" was displayed. The laser stimulation to suppress vmPFC PV neurons was given in the time frames where "Laser on" was displayed.

paired t test), but it is not significantly different from the latency of the rest of inhibition trials (**Figure 5—Figure supplement I,J,** p = 0.0943, paired t test). The latency of the first non-inhibited trial following an inhibition block is significantly different from the latency of the preceding inhibition trials (**Figure 5—Figure supplement K,L,** p = 0.0343, paired t test) but is not significantly different from the latency of subsequent non-inhibited trials (**Figure 5—Figure supplement K,L,** p = 0.8147, paired t-test). These results suggest that vmPFC PV neuronal activity plays a causal role in modulating ongoing behavior.

To further tease apart the role of vmPFC PV neural activity in learning, we inhibited vmPFC PV neurons for 2 seconds only after successful chamber crossings in the avoidance task (**Figure 5—Figure supplement M**), a manipulation that did not affect behavioral score on the current trial (**Figure 5—Figure supplement N-P**). With this experimental design, speed was not affected by vmPFC PV inhibition (**Figure 5—Figure supplement P**, no significant interaction between opsins and stimulation was found, p = 0.8846, 2-way ANOVA). The latency of the first trials in the inhibition blocks showed no significant difference from the latency of the second trials in inhibition blocks (**Figure 5—Figure supplement Q**, p = 0.6944, paired t-test), and the latency of the first trials after the end of the inhibition block also showed no difference to the latency of the second trials after the inhibition block (**Figure 5—Figure supplement Q**, p = 0.6745, paired t-test). Thus, post-avoidance inhibition of vmPFC PV neural activity did not affect avoidance latency in subsequent trials.

DISCUSSION

Here, we show that vmPFC PV neural activity rises during movements to avoid cued impending shocks, unexpected given the established role of the vmPFC in fear extinction and the inhibitory nature of PV neurons. Inhibiting vmPFC PV neural activity delayed avoidance and prolonged freezing, demonstrating that vmPFC PV neurons are critical for initiating an adaptive defensive response. This elevated activity is not velocity-, latency- or outcome-dependent, and was only observed during adaptive defensive movements. vmPFC PV neural activity was not elevated during movements toward reward or during general locomotion, nor were these behaviors affected by manipulation of vmPFC PV neurons.

The importance of vmPFC PV neural activity in adaptive defensive may be due to the requirement for suppressing environment-specific prepotent behavioral responses. vmPFC PV neurons are

recruited to suppress automatic reactions and thus permit proactive and other flexible responses. In avoidance, freezing is the default response of mice upon hearing a shock-predicting tone. When a predator is in the distance, freezing can increase the chance of survival by reducing detection by the predator. However, if time permits, avoidance becomes a better option than freezing by preventing a future encounter with the predator. Reactive freezing must be shut down for adaptive avoidance behavior to be expressed. However, in reward-based tasks there is no automatic freezing response to conflict with reward approach behavior.

Recent studies have suggested that the role of cortical PV neurons may go beyond suppressing overall neural activity in a region. Rather, it rather likely plays a more delicate role in tuning local computation. For example, PV neurons aid in improving visual discrimination through sharpening response selectivity in visual cortex (Lee et al., 2012). In prefrontal cortex, PV neurons are critical for task performance, particularly during performance of tasks that require flexible behavior, such as rule shift learning (Cho et al., 2020) and reward extinction (Sparta et al., 2014). These studies and our findings support the idea that PV neural activity supports the execution of a behavior by filtering conflicting behaviors, each likely mediated by a different subcortical-projecting pyramidal population (Lee et al., 2014; Sleezer et al., 2021; Warden et al., 2012). In proactive defense, vmPFC PV neurons likely suppress pro-freezing vmPFC projection neurons, to enable the freezing-suppressing vmPFC-ITC projection (Berretta et al., 2005; Vertes, 2006, 2004) and vmPFC-BMA projection (Adhikari et al., 2015) to gain control of behavior through mutual inhibition among PV neurons (Berretta et al., 2005; Gibson et al., 1999; Lee et al., 2014; Pfeffer et al., 2013). This may explain why PV neurons are broadly-tuned to multiple events while manipulation of PV neurons has a relatively specific behavioral effect.

Our findings have revealed the role of vmPFC PV neural activity in facilitating proactive defensive behavior. Though only a relatively sparse cortical population, inhibiting these neurons has a clear and specific detrimental effect on the initiation of avoidance behavior, which is vital for leaving a dangerous situation. Our work also suggests that the functional role of PV neurons extends beyond the overall suppression of the function of a brain region. This shift in our understanding vmPFC PV function is essential for assessing the potential and limitations of the PV neurons as a therapeutic entry point for psychiatric disorders (Donegan and Lodge, 2017; Marín, 2012; Quirk et al., 2009; Thaweethee-Sukjai et al., 2019; Tripp et al., 2012; Wang et al., 2014; Zhang and Reynolds, 2002; Zhou et al., 2015) and provides a conceptual framework of potential utility for

deepening our understanding of the functional roles of PV neurons in mediating conflicting actions through coordination of local circuity under changes in conditions.

MATERIALS AND METHODS

Animals

All procedures conformed to guidelines established by the National Institutes of Health and have been approved by the Cornell University Institutional Animal Care and Use Committee. PV-Cre mouse line (B6.Cg-Pvalbtm1.1(cre)Aibs/J, RRID:IMSR_JAX:017320) acquired from The Jackson Laboratory (Bar Harbor, ME) was backcrossed to C57BL/6J mice (RRID:IMSR_JAX:000664). Postnatal six weeks to ten months PV-Cre mice were used for photometry and optogenetics experiments. All mice were housed in a group of two to five under 12-hour reverse light-dark cycle (dark cycle: 9 a.m.-9 p.m.).

Viral Vectors

In the photometry experiment, we used AAV1-CAG.Flex.GCaMP6f (Titer: 1.33×10^{13}, Penn Vector Core, 100835-AAV1, Philadelphia, PA) for experimental animals and AAV9-CAG.Flex.GFP (Titer: 3.7×10^{12}, UNC Vector Core, Chapel Hill, NC) for control. All the viral vectors used in photometry experiment were diluted in 8-folds phosphate-buffered saline (PBS) before injection. In the optogenetics experiment, we used AAV5-EF1α-DIO-eNPHR3.0 (Titer: 4×10^{12}, UNC Vector Core, Chapel Hill, NC) for experimental animals and AAV5-EF1α-DIO-EYFP (Titer: 6.5×10^{12}, UNC Vector Core, Chapel Hill, NC) for control. All the viral vectors used in optogenetics experiment were used without dilution.

Surgical Procedures

Mice were put under deep anesthesia with isoflurane (5%). Fur above the skull was trimmed, and the mice were placed in a stereotaxic frame (Kopf Instrument, Tujunga, CA) with a heating pad to prevent hypothermia. Isoflurane level was kept between 0.8 to 2% throughout the surgery. Ophthalmic ointment was applied to protect the eyes. 100 ul 1 mg/ml Baytril (enrofloxacin) was given subcutaneously, and 100 ul 2.5 mg/ml bupivacaine was injected subdermally at the incision site. The scalp was disinfected with betadine and alcohol. The skull was exposed with a midline incision. A craniotomy was made above the medial prefrontal (mPFC) cortex.

For fiber photometry animals, virus (AAV1-CAG-Flex-GCAMP6f) was injected into mPFC unilaterally, with half of the animals into the right hemisphere and half of the animals into the left hemisphere (infralimbic cortex (IL) coordinates: -1.55 AP, ±0.3 ML, -2.8 to -3.2 DV). A total of 800nl diluted vector (1:8 dilution) was injected to each mouse. A virus injected was done with a 10 uL Hamilton syringe (nanofil, WPI, Sarasota, FL) and a 33-gauge beveled needle, and a micro-syringe pump controller (Micro 4; WPI, Sarasota, FL) using slow injection speed (100nl/min). The needle was slowly withdrawn 15 minutes after injection. After injection, a 4-mm or 6-mm-long optic fiber (diameter: 400um, 0.48NA, Doric Lenses, Quebec, Canada) was implanted 0.5 to 1 mm above the injection site.

For optogenetics animals, virus (AAV5-EF1a-DIO-eNpHR3.0, Lot #: 4806G, titer: 4.00×10^{12}; control: AAV5-EF1a-DIO-eYFP, Lot #: 4310J, titer: 6.5×10^{12}, UNC vector core, NC, USA) was injected into mPFC bilaterally (IL coordinates: -1.55 AP, ±0.3 ML, -2.8 to -3.2 DV). 500nl vector was injected into each site on each mouse. After injection, a 4mm to 6mm-long optic fiber (diameter: 200um, 0.22NA, Thorlabs, NJ, USA) was implanted 0.5 to 1 mm above the injection site in a 15-degree angle toward midline (AP=1.55, ML=±1.05 or 1.15, DV=-2.8 or -2.99, 15-degree angle).

After the fiber implant, a layer of metabond (Parkell, Inc., Edgewood, NY) and dental acrylic (Lang Dental Manufacturing, Wheeling, IL) was applied to hold the implant in place. Buprenorphine (0.05 mg/kg), carprofen (5 mg/kg), and lactated ringers (500 μL) were administered subcutaneously after surgery. Photometry recording was done no earlier than three weeks later to allow virus expression.

Fiber Photometry

Fiber photometry was implemented with a fiber photometry console (Doric Lenses, Quebec, Canada). An FC-FC optic fiber patch cord (400 um diameter, 0.48NA, Doric Lenses, Quebec, Canada) was connected to implanted fiber with a zirconia sleeve. 405 nm and 475 nm were measured for calcium-independent and calcium-dependent GCaMP signals and were measured with digital lock-in frequency to the input at 208Hz and 530Hz, respectively. Photometry signals were collected at 12 kHz and filtered with a 12 Hz low pass filter.

For photometry animals, four GCamp6f animals have been through only active avoidance. Seven GCamp6f animals and two GFP control animals were tested in the following order: open field test, reward approach test, reward approach with omission (except two GFP and two GCamp6f animals), active avoidance, active avoidance with shortening and extended tone, active avoidance extinction.

Reward Approach (Photometry)

The reward approach task was performed in a 17.25” W x 6.75” D x 10” H metal rectangular shuttle box (MedAssociates, Fairfax, VT) divided into two equal compartments by Plexiglas semi-partitions, which allows animals to move freely between compartments. A water sprout was located at the end of each compartment, and a syringe pump was connected to the sprout for water delivery. Lick was detected with a contact-based lickometer (MedAssociates, Fairfax, VT). Animals were water restricted prior to training. The body weight was checked daily and was maintained above 80% baseline. Animals were trained to first learn the association between tone and reward-licking at the waterspout in the opposite compartment, by playing a tone for an indefinite length of time (12 kHz or 8 kHz at 70-80 dB, counterbalancing between approach and avoidance) until successful reward collection. When an animal crossed the chamber in response to a tone, water was delivered in the goal compartment, and an indicator light above the targeted water sprout was terminated. After two to three days of training, the reward-indicating lights were removed. Tone duration was set to be turned off either at the chamber crossing or at maximum duration. Animals had to cross within the maximum duration of tone for successful water delivery. The maximum tone duration was shortened as animals progressed and were eventually set to 5 seconds. The inter-trial interval was pseudo-randomized in an average of 40 seconds. Animals were allowed to perform 30-50 trials each day during training and 100 trials on the recording day. The training lasted two to three weeks until animals reach a 70% success rate with a 5-second window. Animals were recorded the day after the criteria were reached for 100 trials.

Reward Approach with 10 % Omission (Photometry)

After well-trained and recorded in reward approach, animals were then switched to a 10% omission paradigm, where water was not delivered on 10% of the successful crossing trials. The omission trials were selected pseudo-randomly at a 10% chance.

Active avoidance (Photometry)

Active avoidance task was performed in a 14” W x 7” D x 12” H metal rectangular shuttle box (Coulbourn Instruments, Holliston, MA) divided into two equal compartments by Plexiglas semi-partitions. Animals were habituated in the chamber for at least 30 minutes, the day before training. On the first day, animals received five five-second habituation tones and two Pavlovian conditionings (a seven-second tone and a two-second shock at the last two-seconds of tone) prior to avoidance trials. The same frequency and amplitude of tone were used for habituation tones, Pavlovian tones, and avoidance tones (12 kHz or 8 kHz at 70-80 dB, counterbalancing between approach and avoidance). After habituation and Pavlovian trials, the task was switched to avoidance trials where animals could prevent the shock from happening by crossing the chamber within 5 seconds from the onset of the tone. Otherwise, an electrical foot shock (0.3 mA) would be delivered through a grid floor for a 2-second maximum before the animal crossed the chamber to escape the shock. The tone was terminated as animals crossed the chamber or after 7 seconds. The inter-trial interval was pseudo-randomized for an average of 40 seconds. Animals performed 100 avoidance trials per day for two to three days or until reaching 70% successful rate. Photometry was recorded throughout the entire training sessions.

Active avoidance with 10% shortened and extended tones (Photometry)

After the standard active avoidance session, animals were then recorded in an alternated version of active avoidance with 10% shortened and extended tones. The only change in this alternated version was to include 10% trials with shortened tones which were turned off 1.5 seconds regardless, and 10% trials with extended tones, which were extended for 1.5 seconds after a successful avoidance. The shortened and extended trials were selected pseudo-randomly at a 10% chance for each trial. No shock was delivered in any shortened-tone and extended-tone trials.

Open Field Test (Photometry)

A 46 W x 46 L x 30.5 H (cm) white rectangular box made with PVC was used for an open field test. The ambient light was set for each 2-minute block in the order of D(dim)-B(bright)-D-B-D-B-D-B-D-B.

Optogenetics

In the behavioral experiment, two external FC-FC optic fiber patch cord (200 um diameter, 0.22 NA, Doric Lenses, Quebec, Canada) were connected to two implanted fibers, respectively, each with a zirconia sleeve. These patch cords were then connected to a 1x2 fiber-optic rotary joint

(FRJ_1x2i_FC-2FC_0.22, Doric Lenses, Quebec, Canada) for unrestricted rotation and to prevent tangling. Another FC-FC optic fiber patch cord was used to connect rotary joint to a 100mw 594 nm diode-pumped solid-state laser (Cobolt Mambo™ 100 594nm, HÜBNER Photonics, Sweden) for optogenetic stimulation. The power of the laser was programmed by the software and fine-tuned by a continuous filter (NDC-50C-2M, Thorlabs, NJ, USA) to 10mW at the end of the patch cord (~71.59 mW/mm^2 at the end of the implanted fiber). The stimulation timing was controlled by a shutter (SRS470, Stanford Research System, Sunnyvale, CA) and a Master-8 stimulus generator (A.M.P.I., Jerusalem, Israel). In avoidance and approach, a total of 72 trials were divided into 12 alternating blocks (OFF-ON-OFF…), and a 2-second continuous stimulation was delivered 0.5 seconds after the onset of a tone during stimulation blocks. In an open field test, a 32-minute test was divided into eight alternating stimulation blocks (OFF-ON-OFF…), a 2-second continuous stimulation was delivered every 40 seconds during the stimulation blocks.

For optogenetics animals, eight experimental and five controls were tested in the following order: open field test under dim light, reward approach, active avoidance, open field test under bright light.

Reward Approach (Optogenetics)

Animals were trained using the same conditioning and chamber and tested in the same chamber as mentioned in *Reward Approach (Photometry)*. After animals reached the learning criteria (70% success rate with 5-second window), animals were then trained with a patch cord attached for another one to two days to habituate the animals to a patch cord. On the test day, 72 trials were divided into 12 alternating blocks (OFF-ON-OFF……), and a 2-second continuous stimulation was delivered 0.5 seconds after the onset of tone during stimulation blocks, regardless of the behavioral outcome.

Active avoidance (Optogenetics)

Animals were trained using the same conditioning and chamber, and were tested in the same chamber as mentioned in *Behavior Paradigm: Active Avoidance (Photometry).* After animals reached the learning criteria (70% success rate with 5-second window), animals were then trained with a patch cord attached for another 1-2 days to habituate the animals to a patch cord. On the test day, 72 trials were divided into 12 alternating blocks (OFF-ON-OFF……), and a 2-second continuous stimulation was delivered 0.5 seconds after the onset of tone during stimulation blocks, regardless of the behavioral outcome.

Open Field Test (Optogenetics, Dim light)

A 26 W x 48 L x 21 H (cm) clean rectangular rat homecage with mice 'homecage bedding placed in a sound-proof box (MedAssociates, Fairfax, VT) lit by a red LED strip was used for an open field test. Mice were first habituated with their cagemates, food, and water in the arena for an hour the day before testing. During the test, food and water were removed from the arena, and each mouse was tested individually. At the start of the experiment, mice were first connected to the patch cord fiber and then placed in the center of the arena. A 32-minute test was divided into eight alternating stimulation blocks (OFF-ON-OFF……), a 2-second continuous stimulation was delivered every 40 seconds during the stimulation blocks.

Open Field Test (Optogenetics, Bright light)

A 46 W x 46 L x 30.5 H (cm) white rectangular box made with PVC was used for an open field test under bright room light. Mice were first connected to the patch cord fiber and then placed in the center of the arena at the start of the experiment. A 32-minute test was divided into eight alternating stimulation blocks (OFF-ON-OFF……), a 2-second continuous stimulation was delivered every 40 seconds during the stimulation blocks.

Perfusion and Histology Verification

After experiments, animals were deeply anesthetized with pentobarbital at a dose of 90 mg/kg and perfused with 20 ml PBS, followed by 20 ml 4% paraformaldehyde solution. Brains were soaked in 4 °C 4% paraformaldehyde for 20 hours and then switched to 30% sucrose solution for about 20-40 hours until the brains sank. Brains were sectioned coronally (40-50 μm) with a freezing microtome and then washed with PBS and mounted with PVA-DABCO. Images were acquired using a Zeiss confocal with 5x air, 20x water, and 40x water objectives.

Statistics and Data analysis

All data analysis and statistical testing were performed using custom-written scripts in MATLAB 2019 (MathWorks, Natick, MA). For all behaviors, animals 'location and movement were tracked using Ethovision XT10 (Noldus Leesburg, VA).

Error bars and shaded areas in figures report standard error of the mean (s.e.m.). All statistical tests were two-tailed. Within-subject analyses were performed using paired t-test, and between-subject analyses were performed using an unpaired t-test.

Photometry signal analysis

ΔF/F was calculated with equation (Eq. 1). The signal measured from the 405 nm reference channel was linearly fitted to the 475 nm signal and was subtracted from the 475 nm signal. The difference was then divided by an exponential function ($a \cdot e^{-b} + c$) fitted to 475 nm signal.

$$\frac{\Delta F}{F} = \frac{475nmsignal - fitted405nmsignal}{exponentialdecayfittedto475nmsignal} \text{ x } 100 \text{ (Eq. 1)}$$

Open field test analysis

Speed of animals was first grouped into three clusters, nonmovement, low movement, and high movement, using k-means. The movement threshold was thus defined by the lowest speed of the low movement cluster. Then the peak speed of the movement was detected by finding local maxima with absolute peak value larger than a threshold and at least 5 cm/s larger than the baseline. (This was performed using *findpeak* function in MATLAB and with 'MinPeakProminence 'set to 5 and with 'MinPeakHeight 'set to movement threshold.) Movement initiation was defined by when the speed first went above 10% of the peak speed within 2 seconds before the epoch. Only epochs with at least 1 second of less than threshold speed before movement initiation were included. Group photometry analyses compared mean ΔF/F 4 to 2 seconds before and 2 seconds around the peak speak of the movement. Optogenetic analyses compared speed differences of NpHR- and eYFP-expressing mice between mean speed during the 2-second stimulation period and mean speed at 2-second right before the stimulation.

Approach task & Active Avoidance task

Group Photometry Analysis

Group photometry analyses compared mean ΔF/F 4 to 2 seconds before and 1 second before and after chamber crossing, only successful trials where animals crossed the chamber within a 5-second window were included. In an active avoidance task, movement initiation was defined by when the speed first went above 10% of the speed at the chamber crossing within 2 seconds before the chamber crossing. In Figure 1 - Figure Supplement F, G and H, the maximal ΔF/F around crossing was calculated by taking the maximum ΔF/F from 0.5 seconds before to 1 second after avoidance chamber crossing of each trail, and the corresponding maximal speed around crossing was calculated by taking the maximum speed 0.5 seconds before and after avoidance chamber crossing.

Movement Detection

Movement epochs in habituation and inter-trial intervals in avoidance tasks were detected by finding local maxima with absolute peak value larger than 10 cm/s and at least 3 cm/s larger than the baseline in smoothed speed traces. This was performed using *findpeak* function in MATLAB and with 'MinPeakProminence 'set to 3 and with 'MinPeakHeight 'set to 10. The speed traces were smoothed with Gaussian-weighted moving average with a window of seven frames by MATLAB function *smoothdata* before the movement epoch detection. (The video was recorded in 15 frames per second). The movement was excluded if it happened within 5 seconds after another movement. Habituation was defined as the time starting from when the animals were placed in the chamber to the start of the first Pavlovian conditioning trials on the first day of training.

Movement in the intertrial intervals was measured from 5 seconds after the end of the trials to 5 seconds before the start of the next trials in a well-learned session. Movement initiation was defined by when the speed first went above 10% of the peak speed within 2 seconds before the epoch.

Group Optogenetic Speed and Crossing Probabilities Analysis

Optogenetic speed analyses compared speed differences of NpHR- and eYFP-expressing between mean speed during the 2-second stimulation period (0.5 seconds to 2.5 seconds from the tone onset) in stimulation trials to stimulation period in non-stimulation trials. Trials in which animals crossed before 0.5 seconds after tone onset or before the laser stimulation onset were excluded for speed analyses (Figure 5 D-E, 5H-I and Figure 5-Figure Supplement A and C). To plot a histogram of crossing probabilities under optogenetic stimulation, we first binned the crossing latency of all trials into 0.25-second bins ranging from 0 to 7 seconds and then normalized by the total number of trials to get crossing probability. Optogenetic crossing probability analyses compared differences between NpHR- and eYFP-expressing mice in crossing probability during the 2-second stimulation period (0.5 seconds to 2.5 seconds from the tone onset) in stimulation trials to non-stimulation trials.

Group Optogenetic Block Structure Analysis

In Figure 5-Figure Supplement (I-L), total of 72 active avoidance trials with 12 off-on alternating stimulation blocks, pattern described in Figure 5A, were sectioned into 6 chunks, each chunk

contains 6 trials before stimulation and 6 trials with stimulation. Each data point at each time point is the average latency across 6 chunks of all NpHR-expressing mice. In Figure 5-Figure Supplement (K-L), total of 72 active avoidance trials with 12 off-on alternating stimulation blocks, pattern described in Figure 5A, were then sectioned into 5 chunks, each chunk contains 6 trials with stimulation and 6 trials after stimulation (Due to the stimulation pattern, first “off” block and last “on” block were not included). Each data point at each time point is the average latency across 5 chunks of all NpHR-expressing mice. In Figure 5-Figure Supplement Q, a total of 72 active avoidance trials were sectioned into five chunks; each chunk contains three trials before stimulation, six trials with stimulation, and three trials after stimulation. Each point plotted on the graph is the average across five chunks and of all NpHR-expressing animals.

Freezing Detection

Freezing is detected from video based on changes in pixels by a MATLAB function written by David A. Bulkin and Ryan J. Post. To detect the freezing of animals, we used the code first to convert the video into grayscale, crop the window to include only the bottom of the chamber, and then set the pixels belonging to a mouse to 1s through thresholding pixel values below 27 out of 255. Once the pixels belonging to a mouse are assigned, the code compares the number of pixels changed between frames to get raw movement data. Raw movement data is then filtered with a bandpass filter between 0.01 and 0.9 to ensure the frequency of switching between freezing and non-freezing states matches with the behavior observed. Freezing is then marked when less than 190 mouse pixels were changed in filtered movement data. For Figure 5-Figure Supplement H, duration of freezing was calculated by the total number of frames when the animals were detected freezing during the avoidance latency.

Cross-covariance between photometry signals and speed

Photometry signals were first filtered by a lowpass IIR filter with half-power frequency at 7 Hz and then interpolated to match video recording timeframes (15 Hz). Each segment includes photometry and speed data from 5 seconds after tone offset to 5 seconds before the next tone onset. Cross-covariance was calculated with an offset of ± 2 seconds for each segment by *xcov* function in MATLAB. The cross-covariance value with the largest absolute value within the offset range was selected to be the cross-covariance value of the segment (Seo et al., 2019).

Linear regression model

Calcium signal was modeled as a linear combination of characteristic neural responses to each sensory or action events following the schemes of Musall et al. (2019) and Parker et al. (2016). These events included tone onset, tone offset, avoidance, escape, shock onset, and chamber crossing in the intertrial intervals. The model can be written as in the following equation, where $\Delta F/F$ (t) is the recorded calcium dynamics at time t, k_i and j_i are the kernel coefficients of event type I, τ is the relative time points in a kernel, n1 is the total number of action events, and n2 is the total number of sensory events. For action events, including avoidance, escape, and chamber crossing in intertrial intervals, we used kernels (k_i) ranging from 1 second before to 2 seconds after the event to cover the action from initiation to termination. For sensory events, including tone onsets, tone offsets, and shock onsets, kernels (j_i) started right at the moment where the event happened and lasted for 2 seconds afterwards to model the sensory responses.

$$\Delta F/F(t) = \sum_{i=1}^{n1}\left(\int_{\tau=-1s}^{2s} k_i(\tau) * (t-\tau)d\tau\right) + \sum_{i=1}^{n2}\left(\int_{\tau=0s}^{2s} j_i(\tau) * (t-\tau)d\tau\right) + error \quad \text{(Eq. 2)}$$

Kernel coefficients of the model were solved by minimizing the mean square errors between the model and the actual recorded signals. In the reduced model, either avoidance time points or tone offset time points were shuffled. The coefficients of determination (R^2) was compared between the reduced model and the full model to estimate the unique contribution of certain events to the explanation power of the model. More details of the methods can be viewed in (Musall et al., 2019; Parker et al., 2016).

ACKNOWLEDGMENTS

We thank J.R. Fetcho, R.M. Harris-Warrick, H.K. Reeve, J.H. Goldberg, N. Yapaci, Y. Baumel, W.-K. You, O. Gschwend, W.-S. Wei, W.-C. Huang, J. Cia, T. Zhou, and W. Menegas for helpful discussion, B.J. Sleezer, E. Troconis, A. Guru, R.J. Post and C. Seo for assistance on fiber photometry system and behavioral paradigm, Y. Baumel, C. Seo and B.J. Sleezer for advice on data analysis. This work was supported by Mong Family Foundation (Y.H.), the Taiwan Ministry of Education (Y.H.), NIH DP2MH109982 (M.R.W), the Alfred P. Sloan Foundation (M.R.W.), the Whitehall Foundation (M.R.W.), and the Brain and Behavior Research Foundation (M.R.W). M.R.W. is a Robertson Neuroscience Investigator–New York Stem Cell Foundation.

COMPETING INTEREST STATEMENT

The authors declare no competing interest.

AUTHOR CONTRIBUTIONS

Y.-Y.H. and M.R.W. conceived the idea and designed the experiments. Y.-Y.H., Q.Y. and P.B. initiated and performed the experiments. Y.-Y.H., P.B., D.A.B. and M.R.W. worked on different facets of the data analysis. Y.-Y.H., D.A.B. and M.R.W. wrote the paper, and all authors contributed to the final manuscript.

DATA ACCESSIBILITY

The authors declare that the data supporting the findings of this study are available within the paper, the methods section, and Extended Data files. Raw data are available from the corresponding author upon reasonable request.

REFERENCES

Adhikari A, Lerner TN, Finkelstein J, Pak S, Jennings JH, Davidson TJ, Ferenczi E, Gunaydin LA, Mirzabekov JJ, Ye L, Kim S-Y, Lei A, Deisseroth K. 2015. Basomedial amygdala mediates top-down control of anxiety and fear. *Nature* **527**:179–185. doi:10.1038/nature15698

Berretta S, Pantazopoulos H, Caldera M, Pantazopoulos P, Paré D. 2005. Infralimbic cortex activation increases c-fos expression in intercalated neurons of the amygdala. *Neuroscience* **132**:943–953. doi:10.1016/j.neuroscience.2005.01.020

Bianchi L. 1922. The mechanism of the brain and the function of the frontal lobes. Edinburgh: E. & S. Livingstone.

Cho KKA, Davidson TJ, Bouvier G, Marshall JD, Schnitzer MJ, Sohal VS. 2020. Cross-hemispheric gamma synchrony between prefrontal parvalbumin interneurons supports behavioral adaptation during rule shift learning. *Nat Neurosci* **23**:892–902. doi:10.1038/s41593-020-0647-1

Cui G, Jun SB, Jin X, Pham MD, Vogel SS, Lovinger DM, Costa RM. 2013. Concurrent activation of striatal direct and indirect pathways during action initiation. *Nature* **494**:238–242. doi:10.1038/nature11846

Do-Monte FH, Manzano-Nieves G, Quiñones-Laracuente K, Ramos-Medina L, Quirk GJ. 2015. Revisiting the Role of Infralimbic Cortex in Fear Extinction with Optogenetics. *J Neurosci* **35**:3607–3615. doi:10.1523/JNEUROSCI.3137-14.2015

Donegan JJ, Lodge DJ. 2017. Hippocampal Perineuronal Nets Are Required for the Sustained Antidepressant Effect of Ketamine. *International Journal of Neuropsychopharmacology* **20**:354–358. doi:10.1093/ijnp/pyw095

Duncan J. 1986. Disorganisation of behaviour after frontal lobe damage. *Cognitive Neuropsychology* **3**:271–290. doi:10.1080/02643298608253360

Estebanez L, Hoffmann D, Voigt BC, Poulet JFA. 2017. Parvalbumin-Expressing GABAergic Neurons in Primary Motor Cortex Signal Reaching. *Cell Reports* **20**:308–318. doi:10.1016/j.celrep.2017.06.044

Gibson JR, Beierlein M, Connors BW. 1999. Two networks of electrically coupled inhibitory neurons in neocortex. *Nature* **402**:75–79. doi:10.1038/47035

Giordano N, Alia C, Fruzzetti L, Pasquini M, Mazzoni A, Micera S, Fogassi L, Bonini L, Caleo M. 2021. Fast-spiking interneurons of the premotor cortex contribute to action planning. *bioRxiv* 2021.05.14.443822. doi:10.1101/2021.05.14.443822

Gunaydin LA, Grosenick L, Finkelstein JC, Kauvar IV, Fenno LE, Adhikari A, Lammel S, Mirzabekov JJ, Airan RD, Zalocusky KA, Tye KM, Anikeeva P, Malenka RC, Deisseroth K. 2014. Natural Neural Projection Dynamics Underlying Social Behavior. *Cell* **157**:1535–1551. doi:10.1016/j.cell.2014.05.017

Halladay LR, Blair HT. 2017. Prefrontal infralimbic cortex mediates competition between excitation and inhibition of body movements during pavlovian fear conditioning. *Journal of Neuroscience Research* **95**:853–862. doi:https://doi.org/10.1002/jnr.23736

Hardung S, Epple R, Jäckel Z, Eriksson D, Uran C, Senn V, Gibor L, Yizhar O, Diester I. 2017. A Functional Gradient in the Rodent Prefrontal Cortex Supports Behavioral Inhibition. *Current Biology* **27**:549–555. doi:10.1016/j.cub.2016.12.052

Isomura Y, Harukuni R, Takekawa T, Aizawa H, Fukai T. 2009. Microcircuitry coordination of cortical motor information in self-initiation of voluntary movements. *Nature Neuroscience* **12**:1586–1595.

Koolhaas JM, Korte SM, De Boer SF, Van Der Vegt BJ, Van Reenen CG, Hopster H, De Jong IC, Ruis MAW, Blokhuis HJ. 1999. Coping styles in animals: current status in behavior

and stress-physiology. *Neuroscience & Biobehavioral Reviews* **23**:925–935. doi:10.1016/S0149-7634(99)00026-3
Krypotos A-M, Effting M, Kindt M, Beckers T. 2015. Avoidance learning: a review of theoretical models and recent developments. *Front Behav Neurosci* **9**. doi:10.3389/fnbeh.2015.00189
Lee AT, Gee SM, Vogt D, Patel T, Rubenstein JL, Sohal VS. 2014. Pyramidal Neurons in Prefrontal Cortex Receive Subtype-Specific Forms of Excitation and Inhibition. *Neuron* **81**:61–68. doi:10.1016/j.neuron.2013.10.031
Lee S-H, Kwan AC, Zhang S, Phoumthipphavong V, Flannery JG, Masmanidis SC, Taniguchi H, Huang ZJ, Zhang F, Boyden ES, Deisseroth K, Dan Y. 2012. Activation of specific interneurons improves V1 feature selectivity and visual perception. *Nature* **488**:379–383. doi:10.1038/nature11312
Lhermitte F. 1983. “Utilization behaviour” and its relation to lesions of the frontal lobes. *Brain* **106 (Pt 2)**:237–255. doi:10.1093/brain/106.2.237
Marín O. 2012. Interneuron dysfunction in psychiatric disorders. *Nat Rev Neurosci* **13**:107–120. doi:10.1038/nrn3155
Merchant H, de Lafuente V, Peña-Ortega F, Larriva-Sahd J. 2012. Functional impact of interneuronal inhibition in the cerebral cortex of behaving animals. *Progress in Neurobiology* **99**:163–178. doi:10.1016/j.pneurobio.2012.08.005
Merchant H, Naselaris T, Georgopoulos AP. 2008. Dynamic Sculpting of Directional Tuning in the Primate Motor Cortex during Three-Dimensional Reaching. *J Neurosci* **28**:9164–9172. doi:10.1523/JNEUROSCI.1898-08.2008
Milad MR, Quirk GJ. 2002. Neurons in medial prefrontal cortex signal memory for fear extinction. *Nature* **420**:70–74. doi:10.1038/nature01138
Miller EK, Cohen JD. 2001. An integrative theory of prefrontal cortex function. *Annu Rev Neurosci* **24**:167–202. doi:10.1146/annurev.neuro.24.1.167
Moscarello JM, LeDoux J. 2014. Diverse Effects of Conditioned Threat Stimuli on Behavior. *Cold Spring Harb Symp Quant Biol* **79**:11–19. doi:10.1101/sqb.2014.79.024968
Moscarello JM, LeDoux JE. 2013. Active Avoidance Learning Requires Prefrontal Suppression of Amygdala-Mediated Defensive Reactions. *J Neurosci* **33**:3815–3823. doi:10.1523/JNEUROSCI.2596-12.2013
Mowrer OH, Lamoreaux RR. 1946. Fear as an intervening variable in avoidance conditioning. *Journal of Comparative Psychology* **39**:29–50. doi:10.1037/h0060150
Murphy ER, Dalley JW, Robbins TW. 2005. Local glutamate receptor antagonism in the rat prefrontal cortex disrupts response inhibition in a visuospatial attentional task. *Psychopharmacology* **179**:99–107. doi:10.1007/s00213-004-2068-3
Musall S, Kaufman MT, Juavinett AL, Gluf S, Churchland AK. 2019. Single-trial neural dynamics are dominated by richly varied movements. *Nat Neurosci* **22**:1677–1686. doi:10.1038/s41593-019-0502-4
Nashef A, Cohen O, Perlmutter SI, Prut Y. 2020. Cortical inhibitory network selects cerebellar signals for movement initiation. *bioRxiv* 2020.10.20.346775. doi:10.1101/2020.10.20.346775
Okun M, Lampl I. 2008. Instantaneous correlation of excitation and inhibition during ongoing and sensory-evoked activities. *Nature Neuroscience* **11**:535–537. doi:10.1038/nn.2105
Parker NF, Cameron CM, Taliaferro JP, Lee J, Choi JY, Davidson TJ, Daw ND, Witten IB. 2016. Reward and choice encoding in terminals of midbrain dopamine neurons depends on striatal target. *Nat Neurosci* **19**:845–854. doi:10.1038/nn.4287
Pfeffer CK, Xue M, He M, Huang ZJ, Scanziani M. 2013. Inhibition of inhibition in visual cortex: the logic of connections between molecularly distinct interneurons. *Nature Neuroscience* **16**:1068–1076. doi:10.1038/nn.3446

Pinto L, Dan Y. 2015. Cell-Type-Specific Activity in Prefrontal Cortex during Goal-Directed Behavior. *Neuron* **87**:437–450. doi:10.1016/j.neuron.2015.06.021

Quirk MC, Sosulski DL, Feierstein CE, Uchida N, Mainen ZF. 2009. A defined network of fast-spiking interneurons in orbitofrontal cortex: responses to behavioral contingencies and ketamine administration. *Front Syst Neurosci* **3**:13. doi:10.3389/neuro.06.013.2009

Seo C, Guru A, Jin M, Ito B, Sleezer BJ, Ho Y-Y, Wang E, Boada C, Krupa NA, Kullakanda DS, Shen CX, Warden MR. 2019. Intense threat switches dorsal raphe serotonin neurons to a paradoxical operational mode. *Science* **363**:538–542. doi:10.1126/science.aau8722

Sleezer BJ, Post RJ, Bulkin DA, Ebitz RB, Lee V, Han K, Warden MR. 2021. Tonic activity in lateral habenula neurons promotes disengagement from reward-seeking behavior. *bioRxiv* 2021.01.15.426914. doi:10.1101/2021.01.15.426914

Sparta DR, Hovelsø N, Mason AO, Kantak PA, Ung RL, Decot HK, Stuber GD. 2014. Activation of Prefrontal Cortical Parvalbumin Interneurons Facilitates Extinction of Reward-Seeking Behavior. *J Neurosci* **34**:3699–3705. doi:10.1523/JNEUROSCI.0235-13.2014

Thaweethee-Sukjai B, Suttajit S, Thanoi S, Dalton CF, Reynolds GP, Nudmamud-Thanoi S. 2019. Parvalbumin Promoter Methylation Altered in Major Depressive Disorder. *Int J Med Sci* **16**:1207–1214. doi:10.7150/ijms.36131

Tripp A, Oh H, Guilloux J-P, Martinowich K, Lewis DA, Sibille E. 2012. Brain-Derived Neurotrophic Factor Signaling and Subgenual Anterior Cingulate Cortex Dysfunction in Major Depressive Disorder. *AJP* **169**:1194–1202. doi:10.1176/appi.ajp.2012.12020248

Vertes RP. 2006. Interactions among the medial prefrontal cortex, hippocampus and midline thalamus in emotional and cognitive processing in the rat. *Neuroscience* **142**:1–20. doi:10.1016/j.neuroscience.2006.06.027

Vertes RP. 2004. Differential projections of the infralimbic and prelimbic cortex in the rat. *Synapse* **51**:32–58. doi:10.1002/syn.10279

Wang M, Perova Z, Arenkiel BR, Li B. 2014. Synaptic Modifications in the Medial Prefrontal Cortex in Susceptibility and Resilience to Stress. *J Neurosci* **34**:7485–7492. doi:10.1523/JNEUROSCI.5294-13.2014

Warden MR, Selimbeyoglu A, Mirzabekov JJ, Lo M, Thompson KR, Kim S-Y, Adhikari A, Tye KM, Frank LM, Deisseroth K. 2012. A prefrontal cortex–brainstem neuronal projection that controls response to behavioural challenge. *Nature* **492**:428–432. doi:10.1038/nature11617

Zhang ZJ, Reynolds GP. 2002. A selective decrease in the relative density of parvalbumin-immunoreactive neurons in the hippocampus in schizophrenia. *Schizophrenia Research* **55**:1–10. doi:10.1016/S0920-9964(01)00188-8

Zhou Z, Zhang G, Li X, Liu X, Wang N, Qiu L, Liu W, Zuo Z, Yang J. 2015. Loss of Phenotype of Parvalbumin Interneurons in Rat Prefrontal Cortex Is Involved in Antidepressant- and Propsychotic-Like Behaviors Following Acute and Repeated Ketamine Administration. *Mol Neurobiol* **51**:808–819. doi:10.1007/s12035-014-8798-2

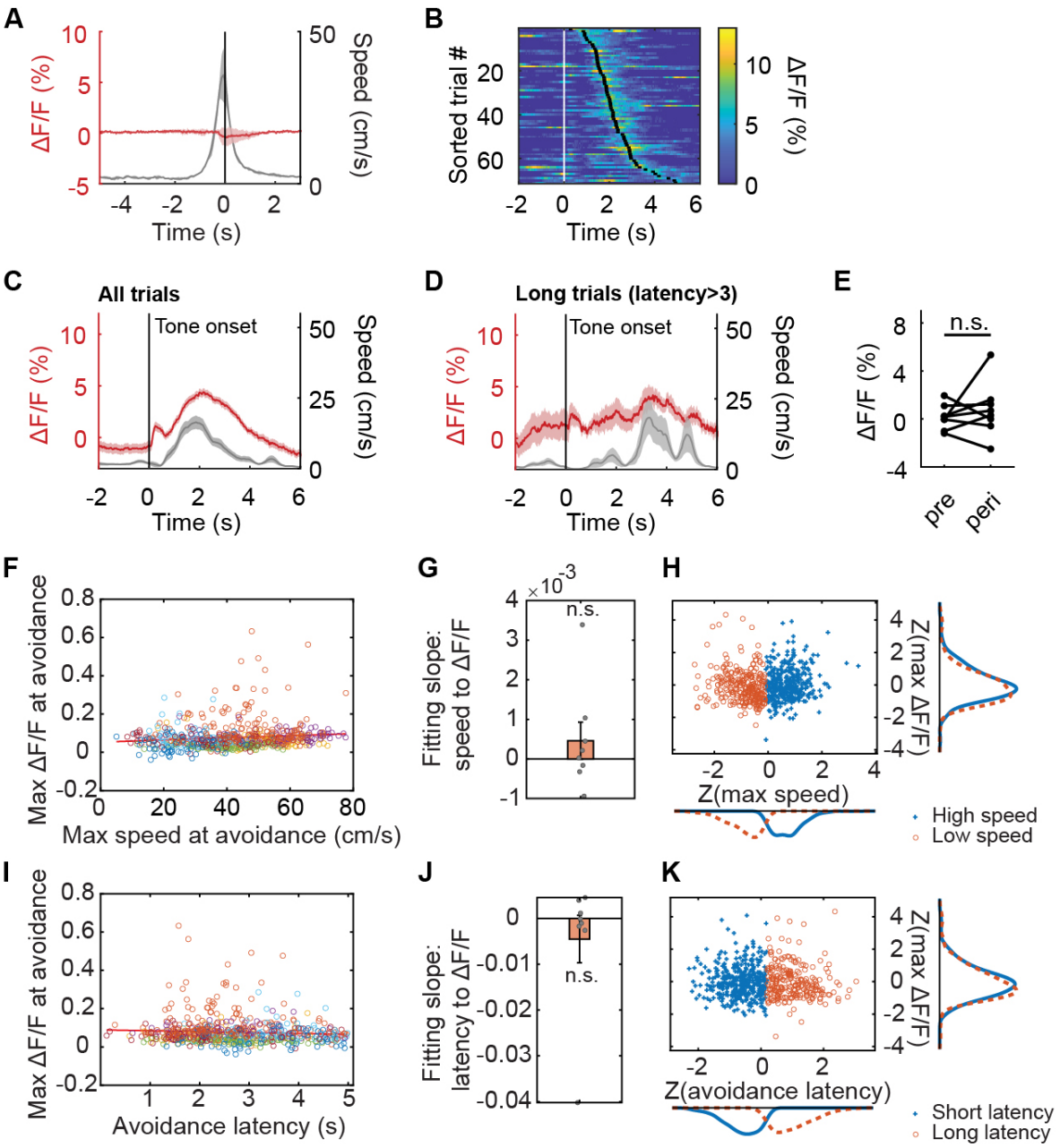

Figure 1—Figure supplement 1.

(A) Average vmPFC PV ΔF/F (red) and speed (grey), aligned to chamber crossing in avoidance from PV::GFP mice. (N=2 mice). (B) vmPFC PV ΔF/F during successful avoidance trials, data aligned to tone onset. White ticks: cue onset. Black ticks: chamber crossing. (C) Example average vmPFC PV ΔF/F (red) and speed (grey), aligned to tone onsets. Same example mouse as B. (D) Example average vmPFC PV ΔF/F (red) and speed (grey) of long latency trials (avoidance latency longer than 3 seconds), aligned to tone onset. Same example mouse as B. (E) Average vmPFC PV ΔF/F before tone onset (pre, 4 to 2 seconds before tone onset) and during tone onset (peri, 0 to 2 seconds after tone onset) of long latency trials (avoidance latency longer than 3 seconds) (N = 8 mice). (F) Correlation between maximum speed and peak vmPFC PV ΔF/F at avoidance. Each dot represents an avoidance trial, and trials from one animal are marked in the same color (N = 8 mice). (G) Distribution of slope of linear correlation between

maximum speed and peak vmPFC PV ΔF/F at avoidance. One dot represents one animal (N = 8 mice). (H) Clustering of distribution of z score of maximum speed and z score of vmPFC PV ΔF/F at avoidance. (I-K) It is the same as (F-H), but the correlation was calculated between avoidance latency and maximum vmPFC PV ΔF/F at avoidance (N = 8 mice). For (E), paired t-test. For (G) and (J), one-sample t-test. Shaded regions indicate SEM.

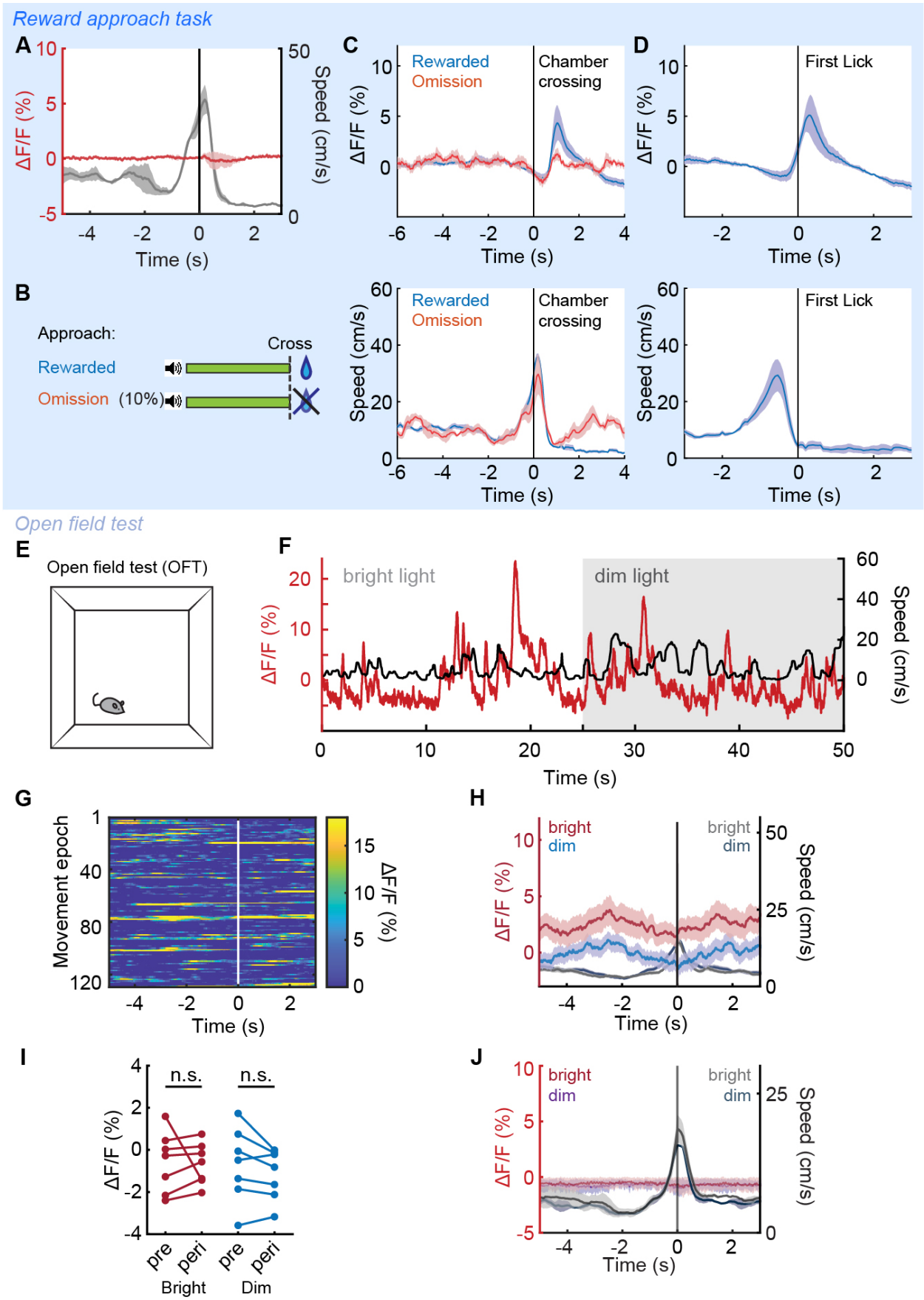
Reward approach task
A
ΔF/F (%)
Speed (cm/s)
Time (s)
B
Approach:
Rewarded
Omission (10%)
Cross
C
Rewarded
Omission
Chamber crossing
D
First Lick
Open field test
E
Open field test (OFT)
F
bright light
dim light
G
Movement epoch
H
bright
dim
I
n.s.
pre
peri
Bright
Dim
J

Figure 3—Figure supplement 1.
(A) Average vmPFC PV ΔF/F (red) and speed (grey), aligned to chamber crossing in approach from PV::GFP mice. (N=2 mice). (B) Schematic of a modified reward approach task with reward omissions. (C) Average vmPFC PV ΔF/F (top) and speed (bottom) of rewarded and omitted trials, aligned to chamber crossing (N=5 mice). (D) Average vmPFC PV ΔF/F (top) and speed (bottom) of rewarded trials, aligned to the first lick after chamber crossing (N=5 mice). (E) OFT schematic. (F) Example vmPFC PV ΔF/F (red) and speed (black) during OFT under interleaving bright lighting (white shading) and dim lighting epochs (grey shading). (G) vmPFC PV ΔF/F during OFT, aligned to maximum speed of each movement epoch in OFT. White ticks: maximum speed of movement epoch. Same example mouse as F. (H) Example average vmPFC PV ΔF/F (red; purple) and speed (grey; dark blue), aligned to maximum speed of each movement epoch in OFT under bright lighting (red; grey) and under dim lighting (purple; dark blue). Same example mouse as F. (I) Average vmPFC PV ΔF/F before movement (pre, 4 to 2 seconds before peak movement) and during movement (peri, 1 second before to 1 second after peak movement) under bright ceiling lighting (red) and dim ceiling lighting (blue) (N = 7 mice). (J) Average vmPFC PV ΔF/F (red; purple) and speed (grey; dark blue), aligned to the maximum speed of each movement epoch in OFT from PV::GFP mice (N=2 mice) under bright lighting (red; grey) and under dim lighting (purple; dark blue). For (I), n.s., $p > 0.05$, paired t-test. Shaded regions indicate SEM.

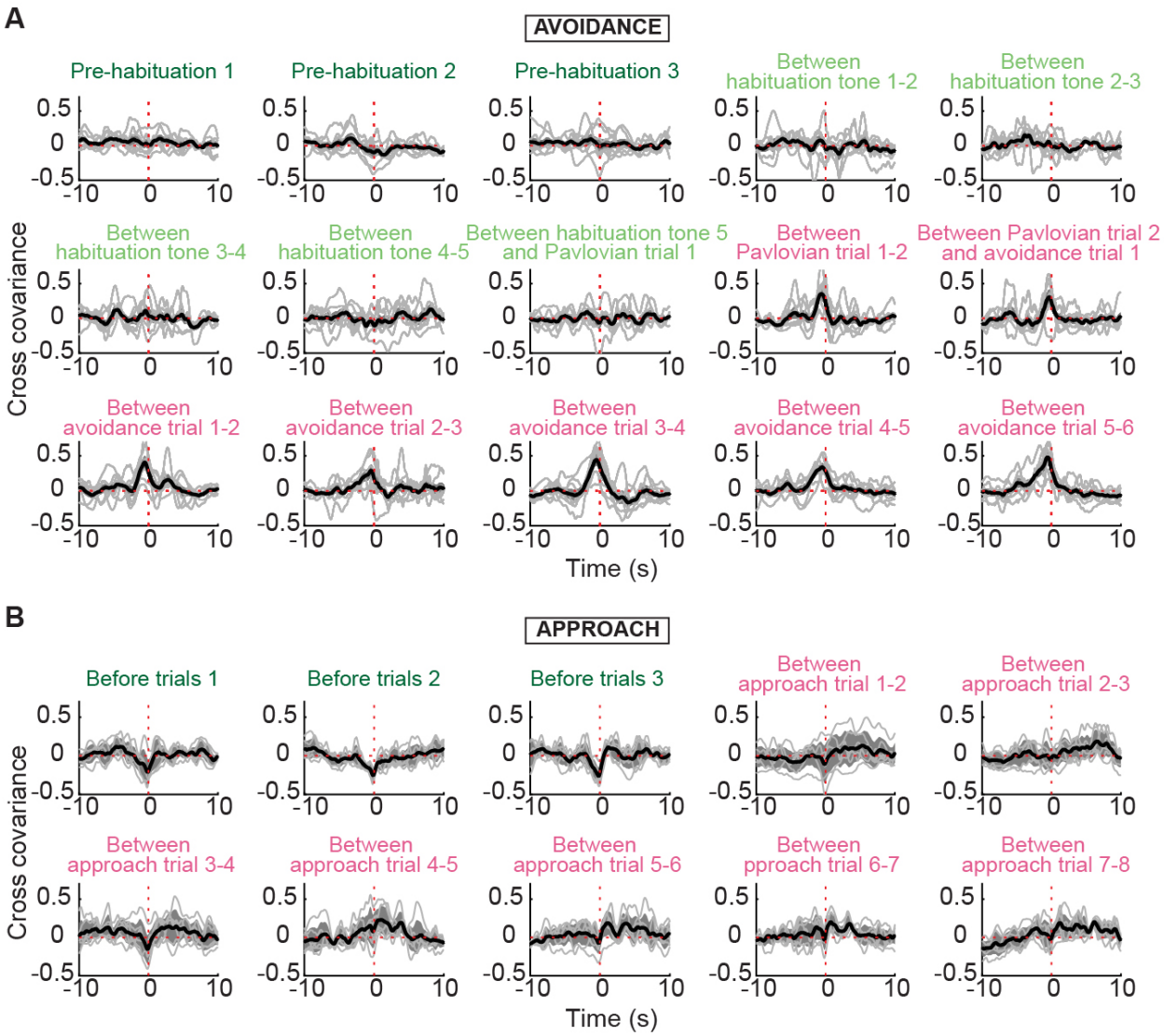

Figure 4—Figure supplement 1. Cross covariance between movement speed and PV activity in avoidance and approach

(A) Evolution of cross-covariance between movement speed and PV activity in habituation and inter-trial intervals on the first day of avoidance training (N=7 mice). (B) Evolution of cross-covariance between movement speed and PV activity in habituation and inter-trial intervals of well-trained animals in an approach task (N=6 mice).

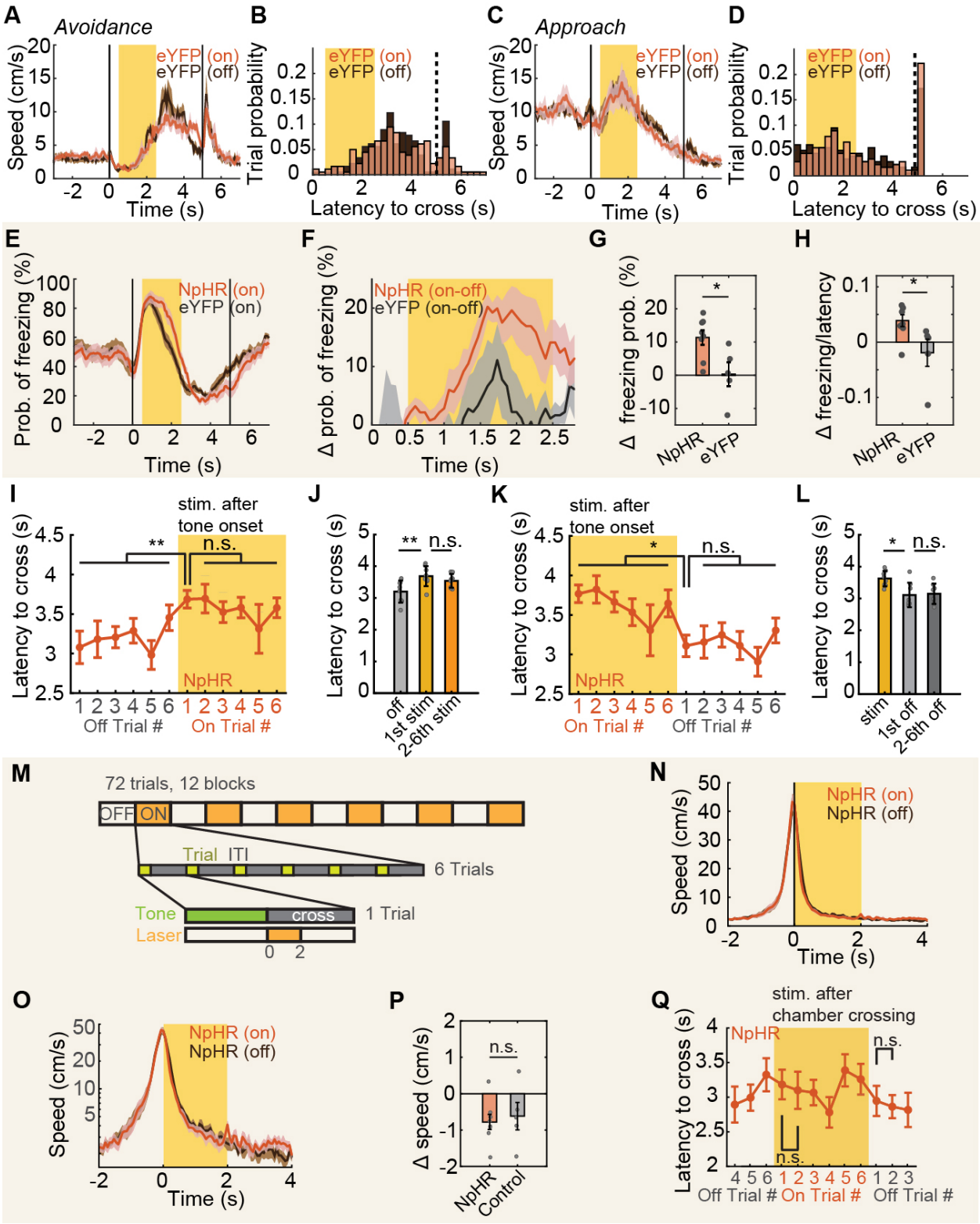

Figure 5—Figure supplement 1. Suppression of vmPFC PV neurons in control animals.
(A) Speed of eYFP-expressing mice during avoidance with (red) and without (dark brown) illumination.
(B) Distribution of crossing latencies during avoidance in eYFP-expressing animals with (red) and without

illumination (brown). (C-D) Same as (A-B) for approach. (E) Freezing probabilities of NpHR-expressing animals during avoidance with (red) and without (dark brown) illumination. (F) Difference in freezing probabilities between with (on) and without (off) illumination in NpHR-expressing mice (red) and in eYFP-expression mice (grey). (G) Difference in freezing probabilities, averaged over the laser stimulation period, between with (on) and without (off) illumination in NpHR-expressing mice (red) and in eYFP-expression mice (grey). (H) Change in ratio of freezing duration/avoidance latency of NpHR-expressing and eYFP-expression mice during illumination compared to non-illumination. (I) Crossing latencies during avoidance in NpHR-expressing mice, grouped by relative position prior or within a stimulation block. (J) Average crossing latencies of all non-illuminated trials (off), 1st trials (1st stim) and 2nd-6th trials in illuminated blocks (2-6th stim). (K) Crossing latencies during avoidance in NpHR-expressing mice, grouped by relative position within or after a stimulation block. (L) Average crossing latencies of all illuminated trials (stim), 1st trials (1st off) and 2nd-6th trials (2-6th off) in non-illuminated blocks. (M) Post-crossing optogenetic inactivation schematic. (N) Speed of NpHR-expressing mice during avoidance with (red) and without (dark brown) illumination. (O) Same as (N), but the y-axis was plotted on a log scale. (P) Change in speed of NpHR-expressing and eYFP-expression mice during illumination (0 to 2 s from avoiding chamber crossing) compared to non-illumination trials. (Q) The latency of the first trials in stimulation blocks is compared to the latency of the second trials in stimulation blocks, and the latency of the first trials after stimulation blocks is compared to the latency of the second trials after stimulation blocks. n.s. $p > 0.05$, $*p < 0.05$, $**p < 0.01$. For (G) and (H), un-paired t-test. For (J), (L) and (Q), paired t-test. For (P), 2-way ANOVA interaction term. Shaded regions indicate SEM. NpHR: N=8 mice, eYFP: N=5 mice.